

LETTER TO THE EDITOR

# Black hole accretion and star formation as drivers of gas excitation and chemistry in Mrk 231

P.P. van der Werf<sup>1\*</sup>, K.G. Isaak<sup>2,3</sup>, R. Meijerink<sup>1</sup>, M. Spaans<sup>4</sup>, A. Rykala<sup>2</sup>, T. Fulton<sup>5</sup>, A.F. Loenen<sup>1</sup>, F. Walter<sup>6</sup>, A. Weiß<sup>7</sup>, L. Armus<sup>8</sup>, J. Fischer<sup>9</sup>, F.P. Israel<sup>1</sup>, A.I. Harris<sup>10</sup>, S. Veilleux<sup>10</sup>, C. Henkel<sup>7</sup>, G. Savini<sup>11</sup>, S. Lord<sup>12</sup>, H.A. Smith<sup>13</sup>, E. González-Alfonso<sup>14</sup>, D. Naylor<sup>15</sup>, S. Aalto<sup>16</sup>, V. Charmandaris<sup>17,29</sup>, K.M. Dasyra<sup>18</sup>, A. Evans<sup>19,20</sup>, Y. Gao<sup>21</sup>, T.R. Greve<sup>6,22</sup>, R. Güsten<sup>7</sup>, C. Kramer<sup>23</sup>, J. Martín-Pintado<sup>24</sup>, J. Mazzarella<sup>12</sup>, P.P. Papadopoulos<sup>25</sup>, D.B. Sanders<sup>26</sup>, L. Spinoglio<sup>27</sup>, G. Stacey<sup>28</sup>, C. Vlahakis<sup>1</sup>, M.C. Wiedner<sup>29</sup>, and E.M. Xilouris<sup>30</sup>

(Affiliations can be found after the references)

Received March 31, 2010; accepted April 27, 2010

## ABSTRACT

We present a full high resolution SPIRE FTS spectrum of the nearby ultraluminous infrared galaxy Mrk 231. In total 25 lines are detected, including CO  $J = 5-4$  through  $J = 13-12$ , 7 rotational lines of H<sub>2</sub>O, 3 of OH<sup>+</sup> and one line each of H<sub>2</sub>O<sup>+</sup>, CH<sup>+</sup>, and HF. We find that the excitation of the CO rotational levels up to  $J = 8$  can be accounted for by UV radiation from star formation. However, the approximately flat luminosity distribution of the CO lines over the rotational ladder above  $J = 8$  requires the presence of a separate source of excitation for the highest CO lines. We explore X-ray heating by the accreting supermassive black hole in Mrk 231 as a source of excitation for these lines, and find that it can reproduce the observed luminosities. We also consider a model with dense gas in a strong UV radiation field to produce the highest CO lines, but find that this model strongly overpredicts the hot dust mass in Mrk 231. Our favoured model consists of a star forming disk of radius 560 pc, containing clumps of dense gas exposed to strong UV radiation, dominating the emission of CO lines up to  $J = 8$ . X-rays from the accreting supermassive black hole in Mrk 231 dominate the excitation and chemistry of the inner disk out to a radius of 160 pc, consistent with the X-ray power of the AGN in Mrk 231. The extraordinary luminosity of the OH<sup>+</sup> and H<sub>2</sub>O<sup>+</sup> lines reveals the signature of X-ray driven excitation and chemistry in this region.

**Key words.** Galaxies: individual: Mrk 231 – Galaxies: active – Galaxies: ISM – Galaxies: nuclei – Galaxies: starburst – Infrared: galaxies

## 1. Introduction

Carbon monoxide (CO) is a fundamental tracer of interstellar molecular gas. However, since only the lowest 3 rotational transitions are relatively easily accessible with ground-based telescopes, the diagnostic use of higher rotational levels is poorly developed. This hiatus in our knowledge is becoming acute now that high- $J$  CO observations of high- $z$  galaxies are becoming possible.

With this in mind, we have embarked on the *Herschel* Comprehensive (U)LIRG Emission Survey (HerCULES), an open time Key Project on the ESA *Herschel* Space Observatory<sup>1</sup> (Pilbratt et al., this issue). The HerCULES project will establish a comprehensive inventory of the gas cooling lines in a flux-limited sample of 29 (Ultra)luminous Infrared Galaxies or (U)LIRGs, using high spectral resolution observations with the Fourier Transform Spectrograph (FTS) of the SPIRE instrument (Griffin et al., this issue), combined with observations of the [C II] 158  $\mu\text{m}$  line and the [O I] 63 and 146  $\mu\text{m}$  lines with PACS (Poglitsch et al., this issue). Key aims of HerCULES are the development of the diagnostic use of the gas cooling lines in local (U)LIRGs, and establishing a local benchmark for observations of high- $z$  galaxies with the Atacama Large Millimeter Array. In addition, since the FTS yields full spectra, any other luminous emission lines detected (e.g., of H<sub>2</sub>O) will be available for study.

\* e-mail: pvdwerf@strw.leidenuniv.nl

<sup>1</sup> *Herschel* is an ESA space observatory with science instruments provided by European-led Principal Investigator consortia and with important participation from NASA.

Spaans & Meijerink (2008) have shown that X-ray excitation of the gas (e.g., by an AGN) and UV irradiation by young massive stars produce very different luminosity distributions over the CO rotational lines. Physically, the difference arises because X-rays penetrate a larger column density of gas than UV photons, and are less effective in dissociating the molecules. In addition, while the gas heating efficiency in a photon dominated region (PDR) is less than 1%, in X-ray dominated regions (XDRs) this efficiency is 10–50%. As a result, for comparable irradiated energies, XDRs tend to have larger column densities of warmer molecular gas than PDRs, and will produce much more luminous emission in the high- $J$  CO lines. In contrast, PDRs are more efficient than XDRs in heating the dust. X-rays also give rise to significant ionization in the molecular gas and therefore drive an efficient ion-molecule chemistry, leading to pronounced chemical differences between PDRs and XDRs (Meijerink & Spaans 2005). Testing and using these diagnostics is one of the principal aims of the HerCULES project.

In this Letter, we discuss the first results of the HerCULES programme and present the SPIRE FTS spectrum of the nearby ULIRG Mrk 231 (UGC 8058, IRAS F12540+5708), the most luminous galaxy in the Revised IRAS Bright Galaxy Sample (Sanders et al. 2003). Adopting  $z = 0.042170$  as the heliocentric redshift of Mrk 231, correcting for the local flow, and applying a flat 5-year WMAP cosmology ( $H_0 = 70 \text{ km s}^{-1} \text{ Mpc}^{-1}$ ,  $\Omega_\Lambda = 0.73$ ) yields a luminosity distance  $D_L = 192 \text{ Mpc}$ , with 1'' corresponding to 0.856 kpc, as provided by NED<sup>2</sup>.

<sup>2</sup> <http://nedwww.ipac.caltech.edu/>

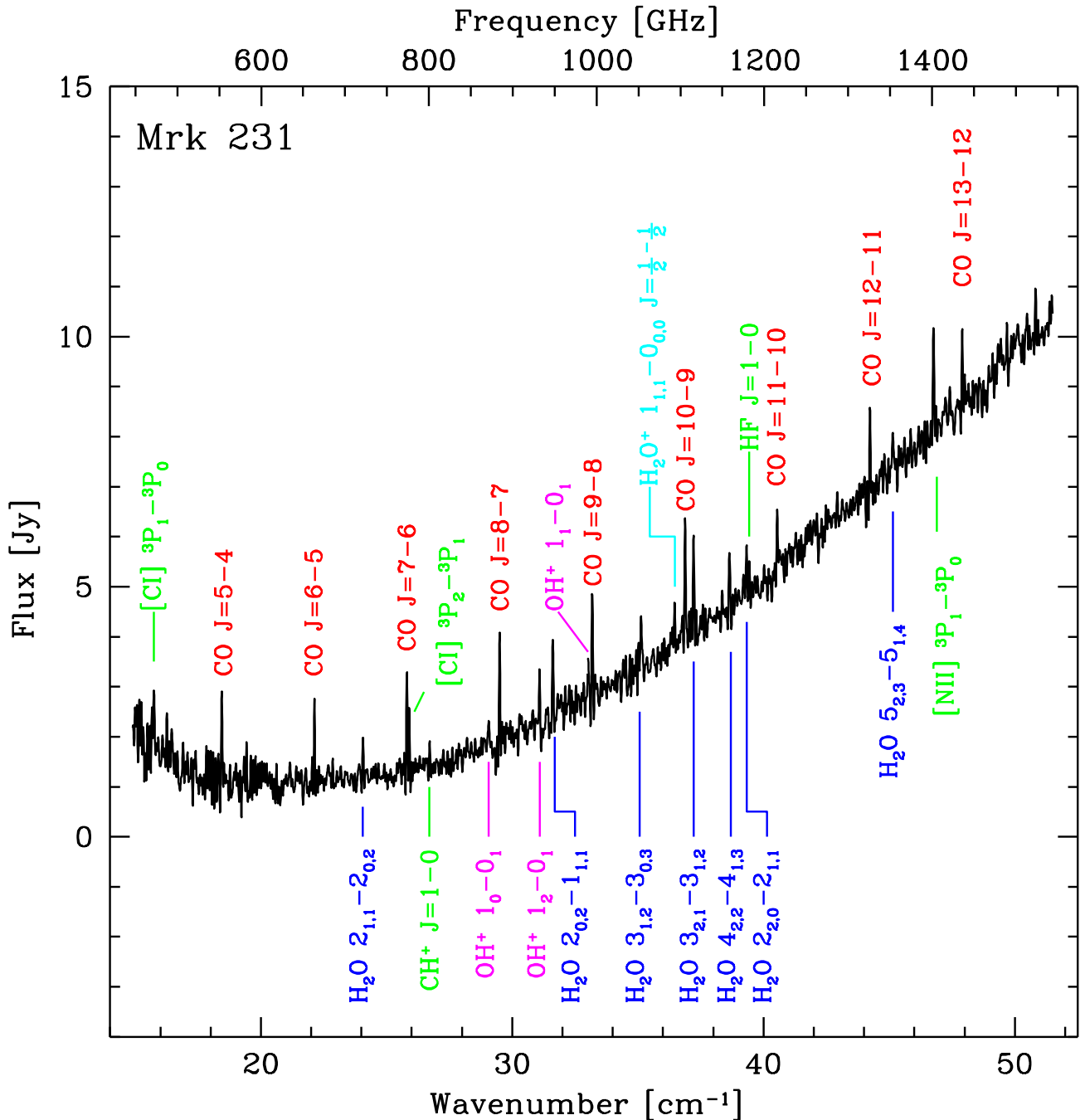


**Fig. 1.** SPIRE FTS spectrum of Mrk 231. Line identifications are given in red for CO lines, in blue for H<sub>2</sub>O, in magenta for OH<sup>+</sup>, in cyan for H<sub>2</sub>O<sup>+</sup>, and in green for the remaining lines.

The derived 8 – 1000  $\mu\text{m}$  luminosity of Mrk 231 is then  $L_{\text{IR}} = 4.0 \cdot 10^{12} L_{\odot}$ . Mrk 231 contains a luminous, optically visible AGN, classified as a Seyfert 1 or a Broad Absorption Line QSO (Boksenberg et al. 1977). A highly absorbed power-law X-ray spectrum was observed by Braitto et al. (2004) with  $L_{\text{X}} = 6^{+0.6}_{-0.3} \cdot 10^{43} \text{ erg s}^{-1}$  between 2 and 10 keV. However, Mrk 231 also contains a kpc size disk harbouring intense star formation as shown by high resolution radio imaging (Taylor et al. 1999). Interferometric imaging of CO  $J = 1-0$  and  $J = 2-1$  emission shows an inner disk of radius  $\sim 520$  pc, containing 45% of the total molecular gas mass, and embedded in a more extended and diffuse emission component; the total molecular gas mass is

$5 \cdot 10^9 M_{\odot}$  (Downes & Solomon 1998). The lowest part of the CO ladder (up to  $J = 6-5$ ), was analysed by Papadopoulos et al. (2007), who showed that the integrated CO emission can provide a significant contribution to the total gas cooling. Indications for X-ray-driven chemistry have been found by Aalto et al. (2007) in HNC and HCN line ratios, and by González-Alfonso et al. (2008) in the abundances of OH and H<sub>2</sub>O observed in absorption with ISO. In a comprehensive study of ULIRGs and low- $z$  quasars, Veilleux et al. (2009) derive a fraction of  $70 \pm 15\%$  for the AGN contribution to the far-infrared luminosity of Mrk 231, with the remainder coming from star formation.

## 2. Observations, data reduction and results

Mrk 231 was observed in staring mode with the SPIRE FTS on December 9, 2009, as part of the *Herschel* Science Demonstration Program. The high spectral resolution mode was used, yielding a resolution of  $0.04 \text{ cm}^{-1}$  over both observing bands: the long wavelength band covering  $14.9\text{--}33.0 \text{ cm}^{-1}$  ( $\lambda = 671\text{--}303 \text{ }\mu\text{m}$ ,  $\nu = 467\text{--}989 \text{ GHz}$ ) and the short wavelength band covering  $32.0\text{--}51.5 \text{ cm}^{-1}$  ( $\lambda = 313\text{--}194 \text{ }\mu\text{m}$ ,  $\nu = 959\text{--}1544 \text{ GHz}$ ). In total 50 repetitions (100 FTS scans) were carried out, yielding an on-source integration time of 6660 s. A reference measurement comprised of 120 repetitions was used to subtract the combined emission from the sky, the telescope and instrument itself. The data were processed and calibrated (using the asteroid Vesta) as described in Swinyard et al. (this issue). Since the CO extent of Mrk 231 is at most  $2''$  (Downes & Solomon 1998), while the SPIRE beam varies from  $17''$  to  $42''$  over our spectrum, calibration procedures appropriate for a pure point source were adopted, and no corrections for wavelength-dependent beam coupling factors were necessary. Because of the excellent match in the overlap region of the two spectrometer bands ( $32\text{--}33 \text{ cm}^{-1}$ ), the bands were simply averaged in this region.

The full SPIRE FTS spectrum of Mrk 231 is shown in Fig. 1. It shows a total of 25 well detected lines. The full CO ladder is detected with 9 lines from CO  $J = 5\text{--}4$  to  $J = 13\text{--}12$ . In addition, 7 rotational lines of  $\text{H}_2\text{O}$  are detected, and the two [C I] fine structure lines and the [N II] fine structure line, as well as rotational transitions of  $\text{CH}^+$  and HF. Very surprising is the detection of luminous emission from  $\text{OH}^+$  and  $\text{H}_2\text{O}^+$ . While a possible detection of absorption in higher transitions of  $\text{OH}^+$  was reported by González-Alfonso et al. (2008), this is the first astronomical detection of  $\text{H}_2\text{O}^+$  except in comets.

The lines are detected superposed on a continuum which rises towards the short wavelength side, and represents the Rayleigh-Jeans tail of the dust emission in Mrk 231. A small difference in the thermal background between the source and the reference observation manifests itself as a moderate flux excess in the continuum at the longest wavelengths. Line fluxes are not affected by this artefact. For these early observations, no matching observations with the SPIRE photometer, to measure the continuum levels, were carried out. Pending this, quantitative analysis of the continuum is premature and in this Letter we restrict ourselves to the spectral lines.

Before fitting line profiles, we subtracted the continuum emission using a grey-body fit made to the underlying spectral energy distribution (SED). Any remaining large-scale ripples were removed using a polynomial or sine wave fit. Line fluxes were recovered from this baseline-subtracted spectrum by iteratively fitting model line profiles to this spectrum. These model line profiles are the convolution of the FTS full resolution instrumental response (a sinc function) with the underlying Gaussian line profile of the emission from the galaxy. The systematic uncertainty in the flux scale for the lines is 20–30% over the  $21\text{--}52 \text{ cm}^{-1}$  waveband, but significantly higher below  $21 \text{ cm}^{-1}$  (which will improve when brighter calibration sources become available). We note that the RMS fluctuations in the spectrum are higher than the thermal noise, as a result of a fringe due to a standing wave in the instrument, which affects the accuracy of the derived parameters for the faintest lines in the spectrum. The removal of this fringe, together with a search for additional faint lines, is the subject of ongoing work.

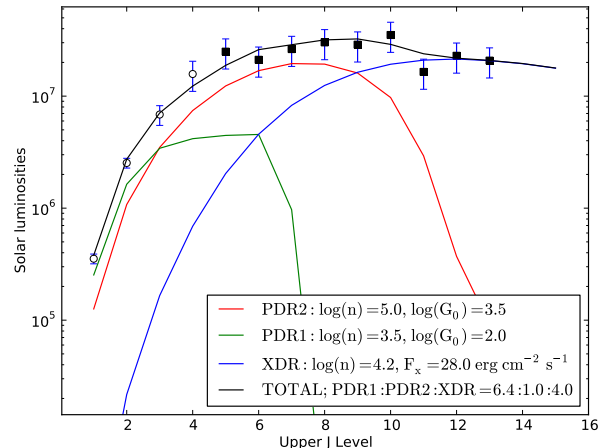


**Fig. 2.** Luminosities of CO lines from Mrk 231. Filled symbols represent measurements from the SPIRE FTS spectrum, while ground-based measurements are denoted with open symbols. Coloured lines indicate two model PDR components (red and green lines) and an XDR component (blue line). The sum of these three components is indicated by the black line and fits the CO measurements. In the legend,  $n$  denotes the number density of hydrogen nuclei ( $n = n_{\text{H}} + 2n_{\text{H}_2}$ ) in  $\text{cm}^{-3}$ ,  $G_0$  denotes the incident UV flux in units of  $1.6 \cdot 10^{-3} \text{ erg s}^{-1} \text{ cm}^{-2}$  for the PDRs, and  $F_{\text{X}}$  the incident X-ray flux for the XDR. The legend also indicates the relative emitting areas of the three components.

## 3. Discussion

### 3.1. CO excitation

We combine the CO line fluxes from the spectrum shown in Fig. 1 with ground-based measurements of the lower lines (Papadopoulos et al. 2007, and references therein) in order to construct the CO rotational excitation diagram shown in Fig. 2. It is seen that an approximately flat luminosity distribution is obtained for the lines from  $J = 5$  upwards. Note that the CO  $J = 10\text{--}9$  line is blended with the  $\text{H}_2\text{O}$   $3_{1,2}\text{--}2_{2,1}$  line which is expected to have some luminosity ( $1.8 \cdot 10^7 L_{\odot}$  for the model by González-Alfonso et al., this issue), and this may account for its somewhat high flux. The total luminosity measured in the CO lines up to  $J = 13\text{--}12$  is  $(2.8 \pm 1.1) \cdot 10^8 L_{\odot}$ . Note that only 4% of the total CO line luminosity is contained in the lowest 3 transitions. For comparison, in our Milky Way this fraction is 43% (Fixsen et al. 1999).

The approximately flat distribution of CO line luminosity with rotational level indicates that several excitation components must be present, since individual components always produce a more peaked excitation diagram. We model these components using the one dimensional PDR/XDR models of Meijerink et al. (2007), as shown in Fig. 2. The CO lines up to  $J = 8\text{--}7$  can be produced by a combination of 2 PDRs, in qualitative agreement with the decomposition by Papadopoulos et al. (2007). However, a challenge is presented by the highest CO lines:  $J = 13\text{--}12$  and  $J = 12\text{--}11$ , arising from energy levels 503 and 461 K above the ground state. As shown in Fig. 2, these lines are strongly underproduced by the PDRs dominating the emission in the lower lines, since the resulting gas temperatures are not high enough for significant population of the  $J > 10$  levels. These lines therefore require the presence of a third excitation component, which can be either an XDR or a high excitation PDR.

A model fit with an XDR producing the highest CO lines is shown in Fig. 2. The required X-ray illumination for this XDR can be produced by the AGN in Mrk 231 (Braitto et al. 2004), out to a distance of 160 pc from the nucleus, ignoring absorption. The ratio of radiating surfaces in the model shown in Fig. 2 implies an extended low excitation PDR component (green curve), with a less extended and denser central XDR region (blue curve). Dense clouds with a smaller surface, close to massive stars and probably embedded in the more diffuse component, account for the medium excitation component (red curve).

Alternatively, a very dense, high illumination PDR can account for the highest CO lines. A good fit is found with  $n = 10^{6.5} \text{ cm}^{-3}$  and  $G_0 = 10^5$  and a surface ratio from medium to high excitation of 1.0 : 0.03. Here the small surface area for the high excitation PDR indicates a number of small high density clumps in a very strong UV field. Since the radiating surface of the high excitation PDR is about 30× smaller than that of the medium excitation PDR, but its density about 30× larger, the H<sub>2</sub> masses in these two components must be comparable. For an O5 star, the required  $G_0 = 10^5$  is reached at a radius of 0.3 pc. For a star formation rate of 100 M<sub>⊙</sub> yr<sup>-1</sup> and a power law initial mass function with slope -2.35 between masses of 0.3 and 120 M<sub>⊙</sub>, there are  $7.6 \cdot 10^5$  stars of spectral type O5 or earlier in Mrk 231. The total volume with  $G_0 > 10^5$  is then  $8.6 \cdot 10^4 \text{ pc}^3$ , while (for a 520 pc radius disk with 15 pc thickness, following Davies et al. (2004)) the total volume of the gas disk is  $1.3 \cdot 10^7 \text{ pc}^3$ . In other words, in this scenario approximately half of the molecular mass would have to be contained in 0.7% of the total volume, and located within 0.3 pc from an O5 (or hotter) star. Efficient UV heating by the  $G_0 = 10^5$  radiation field would heat the dust in these clumps (in total ~ 50% of the total dust mass in Mrk 231) to a temperature of about 170 K. In contrast, in the XDR model, where dust heating would be less efficient, the dust temperature would only be ~ 70 K (Meijerink & Spaans 2005).

These predictions can be tested by analysing the infrared SED of Mrk 231. González-Alfonso et al. (this issue), found that the hot ( $T = 150\text{--}400 \text{ K}$ ) component in the SED of Mrk 231 accounts for about ~ 20% of the total infrared luminosity, but is produced by only 0.02% of the total dust mass. This result limits the fraction of gas within 0.3 pc from an O5 star in Mrk 231 to much less than the ~ 50% required to produce the highest CO lines with a high excitation PDR. This problem does not exist for the XDR model, which predicts most of the dust to be cooler.

### 3.2. XDR chemistry

The extraordinarily luminous emission from the molecular ions H<sub>2</sub>O<sup>+</sup> and OH<sup>+</sup> reveals the chemical signature of an XDR. Assuming that the emission arises from a disk with 160 pc radius (as derived above), we can derive column densities in the upper levels of the relevant transitions, which results in values  $N_{\text{up}} \sim 3.0\text{--}3.5 \cdot 10^{13} \text{ cm}^{-2}$  for both species. Modeling the nuclear molecular gas disk in Mrk 231 with a radius of 520 kpc and H<sub>2</sub> mass of  $2.2 \cdot 10^9 \text{ M}_{\odot}$  then results in lower limits to the total OH<sup>+</sup> and H<sub>2</sub>O<sup>+</sup> abundances relative to H<sub>2</sub> of  $\sim 2 \cdot 10^{-10}$  in the central 160 pc. Given the short radiative lifetimes (< 60 sec) of the upper levels involved, most H<sub>2</sub>O<sup>+</sup> and OH<sup>+</sup> molecules will be in the ground state, and total abundances will exceed these lower limits by large factors. Such abundances require an efficient and penetrative source of ionization in the molecular gas, since the production of OH<sup>+</sup> is mainly driven by  $\text{H}^+ + \text{O} \rightarrow \text{O}^+ + \text{H}$  followed by  $\text{O}^+ + \text{H}_2 \rightarrow \text{OH}^+ + \text{H}$  and  $\text{H}^+ + \text{OH} \rightarrow \text{OH}^+ + \text{H}$ . In the models considered in Sect. 3.1, the key species H<sup>+</sup> is 2–3 orders of magnitude more abundant in the XDR model than in

the high excitation PDR, and the OH<sup>+</sup> abundance is larger by a comparable amount. A similar argument can be made for H<sub>2</sub>O<sup>+</sup>, which is formed by  $\text{OH}^+ + \text{H}_2 \rightarrow \text{H}_2\text{O}^+ + \text{H}$ .

The extraordinary luminosity of the OH<sup>+</sup> and H<sub>2</sub>O<sup>+</sup> (and to a lesser extent CH<sup>+</sup>) lines in Mrk 231 is underlined by a comparison with the SPIRE spectrum of the Orion bar PDR (Habart et al., this issue), which shows no trace of OH<sup>+</sup> or H<sub>2</sub>O<sup>+</sup>, and only weak CH<sup>+</sup> emission, while in Mrk 231 the lines are only a factor 2–3 fainter than the CO lines. While enhanced cosmic ray fluxes in a starburst environment will increase the degree of ionization and hence the production of OH<sup>+</sup> and H<sub>2</sub>O<sup>+</sup> in a PDR, they do not elevate the temperatures to the level required to produce the highest CO lines (Meijerink et al. 2006). It is thus the combination of strong high- $J$  CO lines and high OH<sup>+</sup> and H<sub>2</sub>O<sup>+</sup> abundances that reveals X-ray driven excitation and chemistry in Mrk 231.

## 4. Outlook

We have shown that the SPIRE spectrum of Mrk 231 reveals both PDR and XDR emission lines, and made a separation of these components. A key goal of the HerCULES project will be using this decomposition for a quantitative separation between star formation and black hole accretion as power sources for the infrared luminosities of dusty galaxies. In the case of Mrk 231, this issue will be addressed in a forthcoming paper (Meijerink et al., in prep.). Data will be obtained as part of the HerCULES program for an additional 28 objects, which will enable us to put the results presented here on a statistically significant footing.

*Acknowledgements.* We thank Ewine van Dishoeck, Xander Tielens, and Thomas Nikola for useful discussions. We especially thank Ed Polehampton, Peter Imhof-Davies and Bruce Swinyard for their help with the FTS data processing. JF thanks MPE for its hospitality. The Dark Cosmology Centre is funded by the DNRF. The following institutes have provided hardware and software elements to the SPIRE project: University of Lethbridge, Canada; NAOC, Beijing, China; CEA Saclay, CEA Grenoble and LAM in France; IFSI, Rome, and University of Padua, Italy; IAC, Tenerife, Spain; Stockholm Observatory, Sweden; Cardiff University, Imperial College London, UCL-MSSL, STFC-RAL, UK ATC Edinburgh, and the University of Sussex in the UK. Funding for SPIRE has been provided by the national agencies of the participating countries and by internal institute funding: CSA in Canada; NAOC in China; CNES, CNRS, and CEA in France; ASI in Italy; MEC in Spain; Stockholm Observatory in Sweden; STFC in the UK; and NASA in the USA. Additional funding support for some instrument activities has been provided by ESA.

## References

- Aalto, S., Spaans, M., Wiedner, M. C., & Hüttemeister, S. 2007, *A&A*, 464, 193  
 Boksenberg, A., Carswell, R. F., Allen, D. A., et al. 1977, *MNRAS*, 178, 451  
 Braitto, V., Della Ceca, R., Piconcelli, E., et al. 2004, *A&A*, 420, 79  
 Davies, R. I., Tacconi, L. J., & Genzel, R. 2004, *ApJ*, 613, 781  
 Downes, D. & Solomon, P. M. 1998, *ApJ*, 507, 615  
 Fixsen, D. J., Bennett, C. L., & Mather, J. C. 1999, *ApJ*, 526, 207  
 González-Alfonso, E., Smith, H. A., Ashby, M. L. N., et al. 2008, *ApJ*, 675, 303  
 Meijerink, R. & Spaans, M. 2005, *A&A*, 436, 397  
 Meijerink, R., Spaans, M., & Israel, F. P. 2006, *ApJ*, 650, L103  
 Meijerink, R., Spaans, M., & Israel, F. P. 2007, *A&A*, 461, 793  
 Papadopoulos, P. P., Isaak, K. G., & van der Werf, P. P. 2007, *ApJ*, 668, 815  
 Sanders, D. B., Mazzarella, J. M., Kim, D.-C., Surace, J., & Soifer, B. T. 2003, *ApJS*, 126, 1607  
 Spaans, M. & Meijerink, R. 2008, *ApJ*, 678, L5  
 Taylor, G. B., Silver, C. S., Ulvestad, J. S., & Carilli, C. L. 1999, *ApJ*, 519, 185  
 Veilleux, S., Rupke, D. S. N., Kim, D., et al. 2009, *ApJS*, 182, 628

<sup>1</sup> Leiden Observatory, Leiden University, P.O. Box 9513, NL-2300 RA Leiden, The Netherlands

<sup>2</sup> School of Physics & Astronomy, Cardiff University, Queens Buildings, The Parade, Cardiff CF24 3AA, UK

<sup>3</sup> ESA Astrophysics Missions Division, ESTEC, P.O. Box 299, NL-2200 AG Noordwijk, The Netherlands

<sup>4</sup> Kapteyn Astronomical Institute, University of Groningen, P.O. Box 800, NL-9700 AV Groningen, The Netherlands

<sup>5</sup> Blue Sky Spectroscopy, Lethbridge, Alberta, Canada

<sup>6</sup> Max-Planck-Institut für Astronomie, Königstuhl 17, D-69117 Heidelberg, Germany

<sup>7</sup> Max-Planck-Institut für Radioastronomie, Auf dem Hügel 69, D-53121 Bonn, Germany

<sup>8</sup> Spitzer Science Center, California Institute of Technology, MS 220-6, Pasadena, CA 91125, USA

<sup>9</sup> Naval Research Laboratory, Remote Sensing Division, Washington, DC 20375, USA

<sup>10</sup> Department of Astronomy, University of Maryland, College Park, MD 20742, USA

<sup>11</sup> Department of Physics & Astronomy, University College London, Gower Street, London WC1E 6BT, United Kingdom

<sup>12</sup> Infrared Processing and Analysis Center, California Institute of Technology, Pasadena, CA 91125, USA

<sup>13</sup> Harvard-Smithsonian Center for Astrophysics, 60 Garden Street, Cambridge, MA 02138, USA

<sup>14</sup> Universidad de Alcalá Henares, Departamento de Física, Campus Universitario, E-28871 Alcalá de Henares, Madrid, Spain

<sup>15</sup> Department of Physics, University of Lethbridge, 4401 University Drive, Lethbridge, Alberta, T1J 1B1, Canada

<sup>16</sup> Department of Radio and Space Science, Onsala Observatory, Chalmers University of Technology, SE 439 92 Onsala, Sweden

<sup>17</sup> University of Crete, Department of Physics, GR-71003, Heraklion, Greece

<sup>18</sup> Service d'Astrophysique, CEA Saclay, Orme des Merisiers, 91191 Gif sur Yvette Cedex, France

<sup>19</sup> Department of Astronomy, University of Virginia, 530 McCormick Road, Charlottesville, VA 22904, USA

<sup>20</sup> National Radio Astronomy Observatory, 520 Edgemont Road, Charlottesville, VA 22903, USA

<sup>21</sup> Purple Mountain Observatory, Chinese Academy of Sciences, 2 West Beijing Road, Nanjing 210008, China

<sup>22</sup> Dark Cosmology Centre, Niels Bohr Institute, University of Copenhagen, Juliane Maries Vej 30, 2100 Copenhagen Ø, Denmark

<sup>23</sup> Instituto Radioastronomie Millimetrica (IRAM), Av. Divina Pastora 7, Nucleo Central, E-18012 Granada, Spain

<sup>24</sup> Centro de Astrobiología (INTA-CSIC), Ctra de Torrejón a Ajalvir, km 4, 28850 Torrejón de Ardoz, Madrid, Spain

<sup>25</sup> Argelander Institut für Astronomie, Auf dem Hügel 71, D-53121 Bonn, Germany

<sup>26</sup> University of Hawaii, Institute for Astronomy, 2680 Woodlawn Drive, Honolulu, HI 96822, USA

<sup>27</sup> Istituto di Fisica dello Spazio Interplanetario, CNR, Via Fosso del Cavaliere 100, I-00133 Roma, Italy

<sup>28</sup> Department of Astronomy, Cornell University, Ithaca, NY 14853, USA

<sup>29</sup> LERMA, Observatoire de Paris, 61 Av. de l'Observatoire, F-75014 Paris, France

<sup>30</sup> Institute of Astronomy and Astrophysics, National Observatory of Athens, P. Penteli, GR-15236 Athens, Greece